

# A flexible hybridized electromagnetic-triboelectric nanogenerator and its application for 3D trajectory sensing

Ji Wan<sup>a</sup>, Haobin Wang<sup>a</sup>, Liming Miao<sup>a</sup>, Xuexian Chen<sup>a,b</sup>, Yu Song<sup>a</sup>, Hang Guo<sup>a,b</sup>, Chen Xu<sup>a,b</sup>, Zhongyang Ren<sup>a</sup>, Haixia Zhang<sup>a,b,\*\*</sup>

<sup>a</sup> National Key Laboratory of Science and Technology on Micro/Nano Fabrication, Institute of Microelectronics, Peking University, Beijing, China

<sup>b</sup> Academy for Advanced Interdisciplinary Studies, Peking University, Beijing, China

## ARTICLE INFO

### Keywords:

Hybridized generator  
Magnetic and conductive PDMS  
Energy harvesting  
3D trajectory sensing

## ABSTRACT

Here, we report a flexible hybridized electromagnetic-triboelectric nanogenerator composed of Polydimethylsiloxane (PDMS), multi-walled carbon nanotube (MWCNT) and NdFeB microparticles. The magnetic and conductive Polydimethylsiloxane (MC-PDMS) is soft and flexible enough so that it can be attached onto unsmooth cloth and human skin by adhesive tape and even sewn on the fabric. It works not only as the flexible magnetic polymer of the EMG, providing electromagnetic induction in the copper coil, but also used as TENG's electrode, conducting tribo-electricity. Therefore as a TENG, it generates peak to peak of open-circuit voltage and short-circuit current at 103 V and 7.6  $\mu$ A respectively, and a maximum power density of 7.3  $\mu$ W/cm<sup>2</sup> at 18.8 M $\Omega$ . At the same time, as an EMG, the corresponding peak to peak voltage, current and maximum power are 1.37 V, 1.03 mA and 0.04 mW/cm<sup>2</sup> at 1 K $\Omega$ , respectively. It can charge a capacitance of 10  $\mu$ F to 3 V in 110 s that is superior to the TENG only and EMG only. Furthermore, it can be utilized for self-powered 3D trajectory sensing which involves the capacity of height information detecting above the coil array. This device shows a great potential for applications in wearable electronics and human-machine fields.

## 1. Introduction

In recent years, by coupling triboelectric effects and electrostatic induction, TENG has been attracting extensive attention due to its excellent performance in energy harvesting and self-powered sensing [1–6]. At the same time, to achieve a higher power density and more application scenarios, on the one hand, TENG has been deeply explored in materials [7–9] and structures [10–15], on the other hand, it has been widely combined with other energy conversion devices, including piezoelectric [16–19], magnetoelectric [20–24], thermoelectric devices [25], solar cells [26,27]. Among which, hybridized electromagnetic-triboelectric nanogenerator is one of the largest branches. Compared with TENGs, electromagnetic generators (EMGs) differ in working principles, output characteristics and frequency dependences [28], which determines that these two generators can be supplementary to each other adapting to all kinds of scenes. For example, the hybridized electromagnetic-triboelectric nanogenerators for scavenging biomechanical energy for sustainably powering wearable

electronics [29], the hybridized electromagnetic-triboelectric nanogenerator for a self-powered electronic watch [30], and the self-powered smart active RFID tag integrated with wearable hybrid generator [31]. However, most of the conventional electromagnetic generators are complex in the structure which requires multiplex manufacturing, and they all employed hard and rigid bulk magnets which made them non-flexible states and difficult to assembly, thus they cannot match with the features of the wearable and portable devices. As a result, only very few positions on human body can make a perfect combination with the hybridized generators. Thus for the nanogenerators based wearable devices aimed at biomechanical energy harvesting and powering electronics, a flexible electromagnetic-triboelectric hybrid nanogenerator with simple structure that can covering unsmooth surface is of great significance.

Beyond that, nanogenerators are not only limited to the field of energy harvesting, it also makes great achievements in the field of self-powered sensors [32–37]. Regarding these aspects, location and displacement sensing are the most common applications [38–40], where

\* Corresponding author. National Key Laboratory of Science and Technology on Micro/Nano Fabrication, Institute of Microelectronics, Peking University, Beijing, China.

E-mail address: [zhang-alice@pku.edu.cn](mailto:zhang-alice@pku.edu.cn) (H. Zhang).

<https://doi.org/10.1016/j.nanoen.2020.104878>

Received 14 February 2020; Received in revised form 14 April 2020; Accepted 22 April 2020

Available online 4 May 2020

2211-2855/© 2020 Elsevier Ltd. All rights reserved.

usually an array of nanogenerators is a necessity that can be used for mapping the object's motion information thereon [41–43]. Detections of motions in two dimensions nowadays are easy to get demonstrated with high precision through advanced manufacturing process and materials. However, obtaining the height information of the object in motion is urgent to be resolved, thus there is no doubt that a nanogenerator that can tell the displacement of components in vertical direction is very meaningful.

In this paper, we demonstrated a flexible hybridized electromagnetic-triboelectric nanogenerator based on MC-PDMS for energy harvesting from human motions and 3D trajectory sensing by electromagnetic induction. The single electrode TENG part worked efficiently by the contact between the MWCNT doped PDMS and the kapton coated FPCB coil. At the same time, the EMG part's output is attributed to the NdFeB doped PDMS whose movement can generate electricity in the copper coil. The MC-PDMS differs from conventional hybridized generators materials in its flexibility, owing to which it can be well attached to wrists, fingers and cloth without much burden to human, what's more, it can even be sewn on fabric to harvest energy from human motions and transducing 3D position information. As for the energy harvesting part, with the size of MC-PDMS at 1.5 cm × 4 cm × 0.2 cm, TENG and EMG can achieve maximum output power of 7.3 μW/cm<sup>2</sup> and 0.04 mW/cm<sup>2</sup> respectively under the stimulation at 4 Hz. As a result, a capacitance of 10 μF can be charged to 3 V in 110 s by the hybridized generator that is superior to the charging effect by TENG only (1.21 V) and EMG only (1.94 V). Furthermore, the 3D trajectory recognition can be realized with the assistance of copper FPCB coil array

by electromagnetic induction effect. By attaching the flexible MC-PDMS on the finger, the plane position and stereoscopic information of which above the array can be easily acquired from the magnetoelectricity in the coil array.

## 2. Results and discussion

### 2.1. Design and materials

The MC-PDMS is composed of PDMS, MWCNT generating the conductivity, and NdFeB microparticles providing the magnetism after a pulsed magnetization at 3.5 T. The weight ratio of PDMS, MWCNT and NdFeB is 1: 0.07: 5. The Schematics of pulsed magnetization of MC-PDMS is presented in Fig. 1a, the MC-PDMS is placed in the middle of coil of the pulsed magnetizer, then a giant pulse current is applied, which makes the coil produce a short but extremely strong magnetic field so that the magnetization is finished.

As shown in Fig. 1b, after the magnetization, MC-PDMS with size of 5 μm will have a magnetism along the magnetic line of force, which can be divided into radial magnetization for electromagnetic generator and thickness magnetization for 3D trajectory sensing in Fig. S1. The flexible and biocompatible polymer PDMS is doped with NdFeB microparticles and MWCNT, as a result of which the MC-PDMS is all-flexible so that it can be bend for over 180°.

Fig. 1c shows the inner structure of the MC-PDMS, in which the NdFeB nanoparticles with sizes under 5 μm and MWCNT with length of 20 μm are distributed in the bulk PDMS. By gauss meter, the MC-PDMS

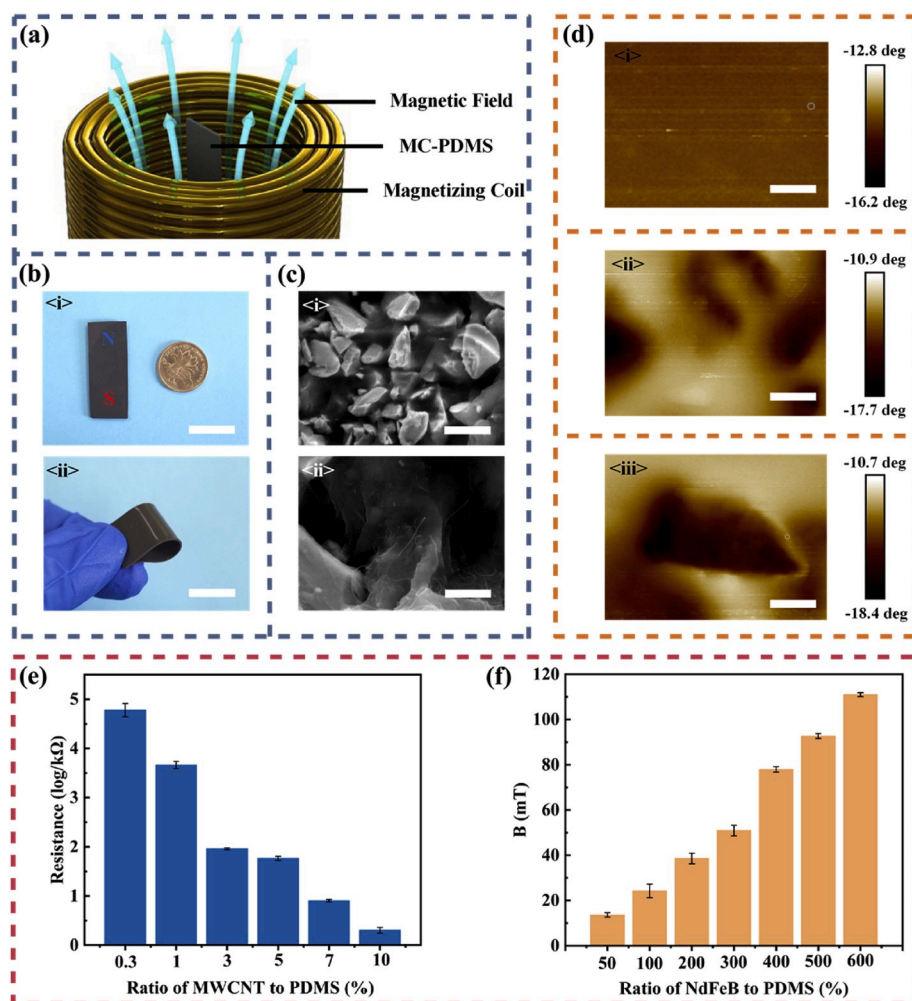


**Fig. 1. Schematics of MC-PDMS.** (a) A schematic illustrating a magnetic PDMS obtained by pulsed magnetization at 3.5 T. (b) Images of the MC-PDMS compared with a coin showing the real size of 1.5 cm × 4 cm × 0.2 cm, and its flexibility. (Scale bar is 2 cm) (c) Scanning electron microscopic images of NdFeB microparticles and MWCNT. (Scale bar is 5 μm and 1 μm respectively) (d) Atomic force microscope images of MC-PDMS <i>i</i> before and <i>ii</i>, <i>iii</i> after pulsed magnetization. (Scale bar is 2 μm, 2 μm and 1 μm, respectively) (e) Resistance of MC-PDMS dependent on the ratio of MWCNT to PDMS. (f) Magnetic induction intensity dependent on the ratio of NdFeB to PDMS.

under radial magnetization can reach a maximum magnetic flux density reaches 92 mT as shown in Fig. S2. To further investigate the magnetization results, we employed Atomic force microscope (AFM) to observe the magnetic domain in the material, the probe was placed 100 nm above the surface and then applied a fixed vibration, which would be influenced by the magnetism of the material in phases. From the AFM images in Fig. 1d there is a strong contrast in MC-PDMS before and after the magnetization and the two poles of the NdFeB particle showing two opposite brightness means that the material is under satisfying magnetization.

Of the materials employed, MWCNT's weight ratio is the key elements deciding the conductivity of the bulk MC-PDMS. Fig. 1e shows that the ratio of MWCNT from 0.3% to 10% will reduce the square resistance of the material from 60 MΩ to 2 kΩ so that it can be more

suitable for a single electrode TENG. As for the magnetism, the amount of the NdFeB's increase will enlarge the maximum magnetic induction intensity of the MC-PDMS measured by the gauss meter as shown in Fig. 1f, as a result of which the EMG can have sufficient output.

### 2.2. Working mode and analysis

The MC-PDMS is magnetic by magnetized NdFeB and conductive by MWCNT, which can work as both a flexible magnet and an electrode of the single-electrode TENG. The structure of the hybrid nanogenerator is illustrated in Fig. 2a in which the MC-PDMS makes a sliding contact with the kapton encapsulated copper coil. As shown in Fig. 2b is the working principle of the TENG. When the kapton touches the MC-PDMS, charges move from kapton to MC-PDMS due to the difference in

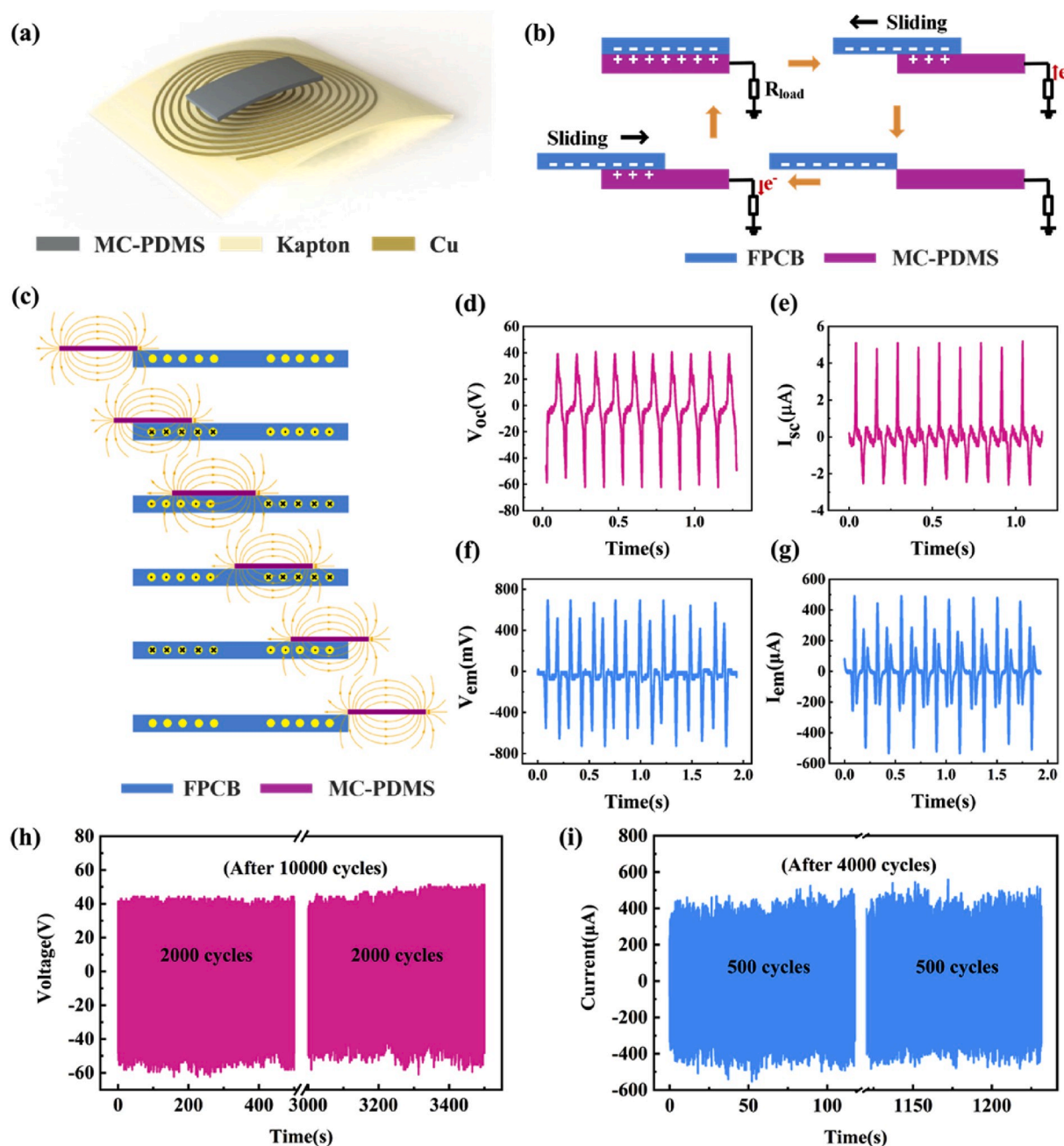


Fig. 2. Working principle and output of the hybridized generator. (a) Structure schematic of the hybridized electromagnetic-triboelectric nanogenerator. Schematic diagram of working principle of (b) TENG and (c) EMG. (d) Output open-circuit voltage and (e) output short-circuit current of TENG under the excitation at 4 Hz. (f) Output voltage and (g) output current of EMG under the excitation at 4 Hz. Cycling reliability of (h) TENG for 14000 cycles and (i) EMG for 5000 cycles.

electronegativity, leading to the kapton positive charged and MC-PDMS negative charged. When the kapton slides outwards, the induced positive charges on the MC-PDMS will decrease, as a result of which the electrons will flow from the ground terminal to the MC-PDMS in order to balance the static charges, thus producing a positive current signal. When the kapton slides all out of the MC-PDMS, the two parts are separated and then an equilibrium state is created without any output. When the kapton slides backwards, the induced positive charges increase, as a result of which the electrons will flow from the MC-PDMS to the ground terminal leading to a negative current signal. Once the two surfaces contact again, the induced charges will meet a maximum value that has no output. Thus repeating process like this will produce steady stream of electricity from the moving of kapton.

While with respect to EMG, Fig. 2c shows the working principle, in

which the MC-PDMS slides above the copper coil. When the MC-PDMS is sliding to the center of the coil, first magnetic induction line will cut the left part of the coil thus having the clockwise current. When the MC-PDMS continues to slide till the north pole over the left part of coil and the south pole over the right part of the coil, there will be anti-clockwise current generating in the coil. Finally, when the MC-PDMS starts to move outwards the coil which means that magnetic induction line near the north pole will cut the right part of the coil thus having a clockwise current again. With this process goes back and forth, electricity will flow continuously across the coil.

Based on the principle mentioned above, the performance of the hybridized generator was evaluated by applying the sliding motion at 4 Hz. As a result, the TENG obtained a peak to peak output open-circuit voltage of 103 V and a peak to peak short-circuit current of 7.6  $\mu\text{A}$ ,

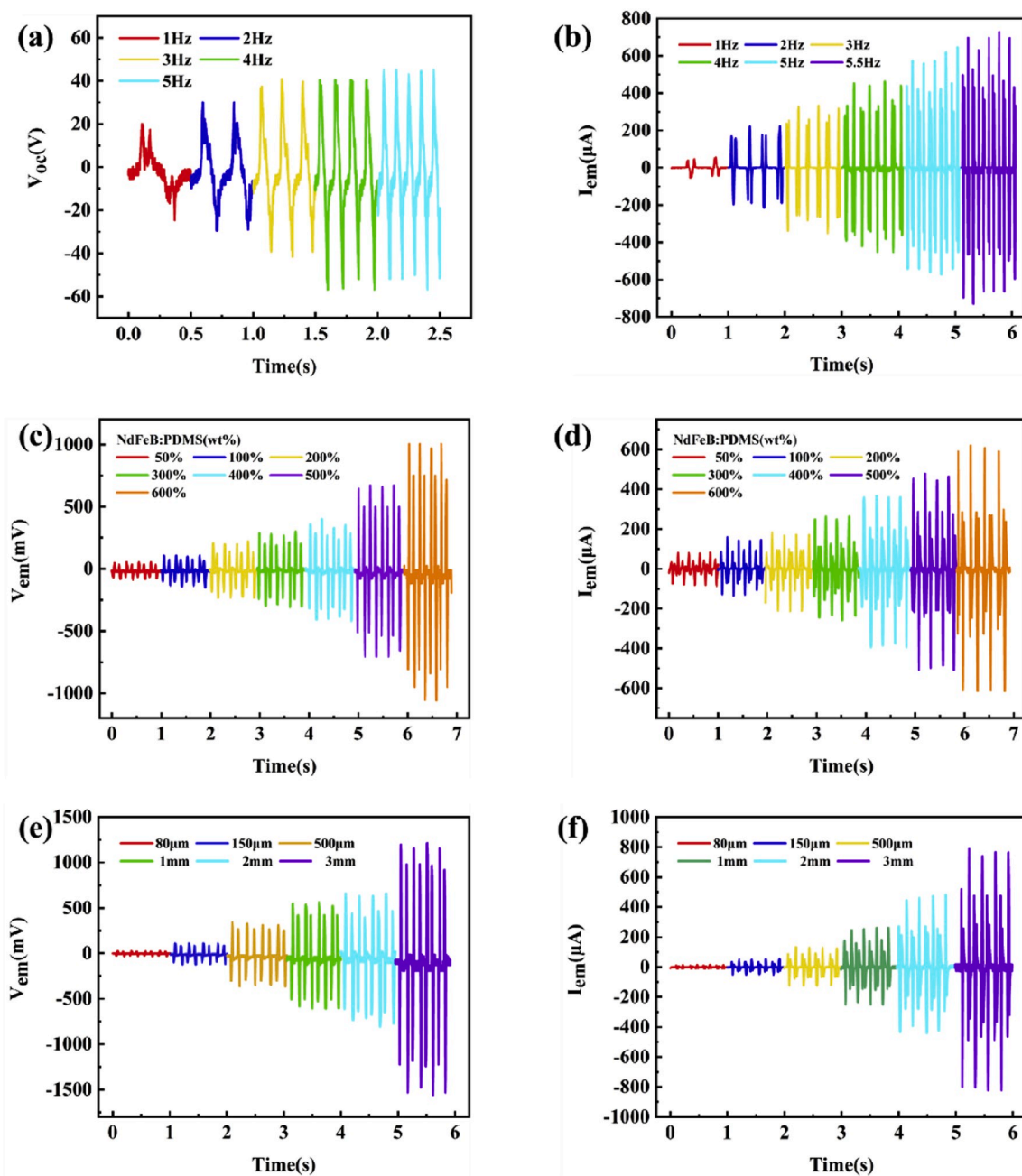


**Fig. 3. Influence factors of the output.** (a) Open-circuit voltage output of TENG at different frequencies. (b) Current output of EMG at different frequencies. (c) Voltage output and (d) current output of EMG at different NdFeB weight ratio. (e) Voltage output and (f) current output of EMG with different thickness of the MC-PDMS.

the EMG obtained a peak to peak of voltage of 1.37 V and a peak to peak of current of 1.03 mA. As is signified in Fig. 2h, the TENG's output can repeat for 14000 cycles with barely no decrease on the signal, at the same time, the EMG's output is also of great stability after 5000 cycles of sliding tests. Also, as shown in Fig. S3 is the wastage of the MC-PDMS during the sliding process. The MC-PDMS have 0.35% weight loss after 10000 cycles of sliding, which means that the hybridized electromagnetic-triboelectric nanogenerator is prepared for numerous numbers of using without any decay in the output and material.

We further compared the MC-PDMS(Wt%<sub>(NdFeB:PDMS)</sub> = 1:5, 9.1 g) with a Fe<sub>3</sub>O<sub>4</sub>(35 g) magnet and a pure NdFeB(12.5 g) magnet as shown in Fig. S4. The MC-PDMS featuring a lighter weight achieved a higher voltage and current output than Fe<sub>3</sub>O<sub>4</sub>, but a lower output than pure NdFeB magnet. MC-PDMS combines flexibility with the strongest magnetic material NdFeB so that it can be used for energy harvesting and wearable devices.

To investigate the MC-PDMS, we further study the influence factor of the hybrid generator's output. First, there is no doubt that the frequencies of the external stimuli applied will make a difference to the output, nevertheless frequency related to human obvious amplitude movement is limited which nearly can't exceed 6 Hz, so stimuli we applied on the hybrid generator is under 6 Hz. The TENG and the EMG share different working principles thus they have different frequency dependence. As for the TENG, the open-circuit voltage can be expressed as:

$$V_{oc} = \frac{Q}{C} \quad (1)$$

Where Q is the transferred charges depending on the materials and the relative area sizes of one contact, C is the capacitance between the MC-PDMS and the kapton, which both bear almost no changes during the sliding process, thus as shown in Fig. 3a when frequency is higher than 4 Hz, the output gradually tends to be stable, instead the relatively low output when frequency is lower than 4 Hz could be attributed to the unstable stimuli forces applied.

While the short-circuit current can be expressed as:

$$I_{sc} = \frac{dQ}{dt} \quad (2)$$

Where  $I_{sc}$  is the short-circuit current of the TENG,  $\frac{dQ}{dt}$  is the transferred charges with time during which MC-PDMS crossing the kapton surface which has a negative relation with the frequency, so the current decreases as shown in Fig. S5a presenting a positive correlation with the frequency.

Besides, with respect to EMG, the voltage output can be expressed as:

$$E = n \frac{d\phi}{dt} = nS \frac{dB}{dt} \quad (3)$$

Where E is the induced electromotive force, n is the turns of the coil,  $\frac{d\phi}{dt}$  is the change of the magnetic flux with time, S is the area size of the coil,  $\frac{dB}{dt}$  is the change of magnetic induction intensity with time, from which a rising frequency leading to change of time will have a rising impact on the output as shown is Fig. S5b. At the same time the current can be expressed as:

$$I = \frac{E}{R} \quad (4)$$

Where I is the current of the EMG, E is the induced electromotive force, R is the resistance of the coil, due to the fact that E is affected by the frequency as shown in Equation (3), the current I of EMG is positive related to the frequency as shown in Fig. 3b.

Besides, as has mentioned above, the MC-PDMS is conductive and magnetic which is MWCNT related and NdFeB related respectively, among which compared the inner resistance of TENG, MWCNT's

resistance at 10 k $\Omega$  is almost negligible. However, the ratio of the NdFeB will directly determine the final magnetization effect leading to different EMG output. As shown in Fig. S6, we doped PDMS with different weight of NdFeB microparticles with NdFeB: PDMS's weight ratio from 50% to 600%, then these MC-PDMS was magnetized in the pulsed magnetizer at 3.5 T. With a 4 Hz sliding stimuli is loaded on the MC-PDMS above the copper FPCB coil, Fig. 3c shows the electromagnetic output voltage corresponding to different NdFeB's doping amount, from which we can see as the NdFeB's weight ratio rising from 50% to 600%, the EMG's peak to peak voltage output increases from 135 mV to 2000 mV which almost has a 1500% increase at the cost of weight. Fig. 3d shows the EMG's current output corresponding to different NdFeB's proportion which also increases from 160  $\mu$ A to 1230  $\mu$ A having a 770% increase. Besides, the flexibility and resistant tearing ability was affected, because the Young's modulus increased as the NdFeB's proportion raised. As shown in Fig. S7, the maximum strain that MC-PDMS can endure decreases from 91% to 20% and the maximum pressure applied till destructive deformation increases from 141 kpa to 510 kpa with the decreasing of NdFeB's percentage, which can be explained by the phenomenon that the MC-PDMS became more 'rigid'.

However, in order to adapt to the application scenarios, output should be considered along with the comfort of human wearable device, so we choose NdFeB: PDMS's weight ratio at 500% which not only has a considerable output but also can be flexible enough for human wearing.

Depart from the NdFeB's weight ratio, the size of the MC-PDMS also makes sense in the application especially the thickness when the length and width is a fixed value at 4 cm and 1.5 cm. Here, we fabricated MC-PDMS with different thickness varying from 80  $\mu$ m to 3 mm by methods of molding. The magnetization effect is closely related to the size of the MC-PDMS, because while employed in the EMG, what produces a marked effect is the magnetic flux which equals magnetic flux density plus the area, as a result, the thickness makes a great contribution to the final output. As shown in Fig. 3e, the thicker the MC-PDMS, the higher the EMG's voltage output, which increases from 60 mV to 2800 mV and the current output increases from 25  $\mu$ A to 1600  $\mu$ A in Fig. 3f. However, among the MC-PDMS samples, the thinner it is, the better it can attach to the object's surface thus we selected the thickness of 2 mm in thickness MC-PDMS which can both make a great EMG output and satisfied the requirement that can be wearable.

### 2.3. Energy harvester

Here, we tested the possibility that flexible MC-PDMS can be wearable as shown in Fig. 4a. The MC-PDMS can be attached to human skin and an unsmooth cloth firmly with adhesive tape, moreover it can be sewn on a fabric with thread piercing the bulk MC-PDMS so that it can be fixed on the clothes, which all seems impossible for the conventional magnet.

Then we at last decided to choose the MC-PDMS with NdFeB: PDMS weight ratio of 500%, thickness of 2 mm and the external stimuli at the frequency of 4 Hz that human can reach while exercising. The MC-PDMS was attached to human without much discomfort in Fig. 4b where MC-PDMS is attached to the wrist band and the copper FPCB coil stuck near the stomach, under the ribs.

People need to swing their arms above their waist in order to balance their body. During the swinging process, with the arms stay close to the body, MC-PDMS will have to make a contact and slide across the coil constantly, thus magnetoelectricity and triboelectricity are generated in the coil and MC-PDMS respectively.

In order to further investigate the energy characteristics of the hybrid generator, we rectified the TENG and the EMG and connect them to a loading resistance and a capacitance as has reflected in Fig. 4c. When the rectified TENG was connected to different resistance, we can tell from Fig. 4d that the voltage output of the TENG increased with the rising external resistance loads while the current output showed a reverse trend, at the same time the voltage output of the EMG also increased and

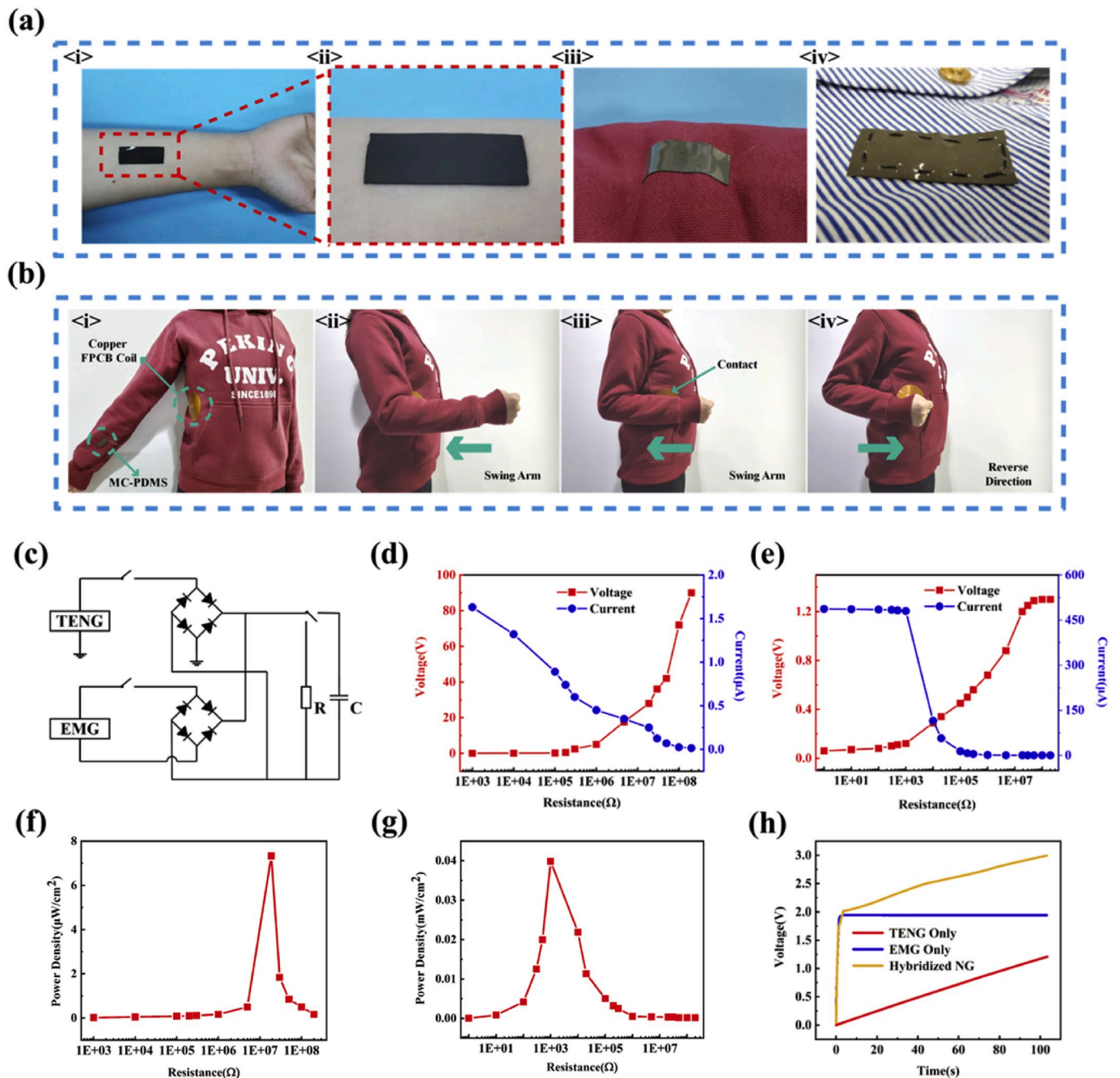


**Fig. 4. Hybrid generator for energy storage.** (a) MC-PDMS attached on <i>, <ii> human skin, <iii> cloth by adhesive tape and <iv> sewn on fabric. (b) Wearable MC-PDMS on the wristband, copper FPCB coil on the coat and working process on human body (c) Configuration of the rectified circuits to TENG and EMG with external loads. (d) TENG's output voltage and current at load resistance ranging from  $1 \times 10^3$  to  $2 \times 10^8 \Omega$ . (e) EMG's output voltage and current at load resistance ranging from 10 to  $2 \times 10^8 \Omega$ . (f) Instantaneous power density of TENG and (g) EMG by  $P = \frac{I^2 R}{A}$ . (h) Charging behavior of capacitance of 10  $\mu\text{F}$  by TENG only, EMG only and hybridized generator.

the current output decreased with the rising external resistance load as shown in Fig. 4e which can be easily explained by Ohm's Law. According to the impedance matching characteristics, the power density can be evaluated by the equation:

$$P = \frac{I^2 R}{A} \quad (5)$$

Where P is the power density, I is the current output of the TENG or EMG, R is the resistance of the external loads and A is the surface area of the MC-PDMS.

Fig. 4f shows the variation of the power density of the TENG across

the external loads and finally a maximum output power density of  $7.3 \mu\text{W}/\text{cm}^2$  with  $18.8 \text{ M}\Omega$  external resistance is achieved. As to the EMG part, the power density achieved a maximum value of  $0.04 \text{ mW}/\text{cm}^2$  with the external resistance of  $1 \text{ k}\Omega$  as shown in Fig. 4g.

Furthermore, the output of the hybrid generator was demonstrated to charge a  $10 \mu\text{F}$  capacitance through rectifier, which is plotted in Fig. 4h. The TENG can charge the capacitance to 3 V in 300 s in Fig. S8a, and the EMG can charge the capacitance to 2 V in 3.5 s in Fig. S8b. To conclude, the TENG's charging can be relatively high but the speed is slow, while the EMG shows a reverse trend that the charging speed fast but the final charging effect is limited. Here, we first used EMG to charge

the capacitance to 2 V in a short period of time, then TENG will continue charging so that the 10  $\mu\text{F}$  capacitance can be charged to 3 V in 110 s which tremendously improve the efficiency, so that energy can be harvested and stored from human body.

### 2.4. Active 3D trajectory sensor

EMG is different from the TENG in that contact is not a must for the EMG because electromagnetic induction is based on cutting magnetic

induction line, so as showed in Fig. 5a, even the thickness magnetization MC-PDMS hangs above the coil at the distance of X, still the coil can have magnetolectricity output. Thickness magnetization MC-PDMS differs from radial magnetization MC-PDMS in that the wave of the former one is stable while the latter's wave is dependent on which the pole sliding into the coil first. Fig. 5b shows that at a 4 Hz stimuli, when X varies from 5 mm to 50 mm, still the EMG can have current output from 840  $\mu\text{A}$  to 40  $\mu\text{A}$ , from which we can tell the height of the MC-PDMS, and even when X = 150 mm, EMG can have a current output of 0.35  $\mu\text{A}$  after 40

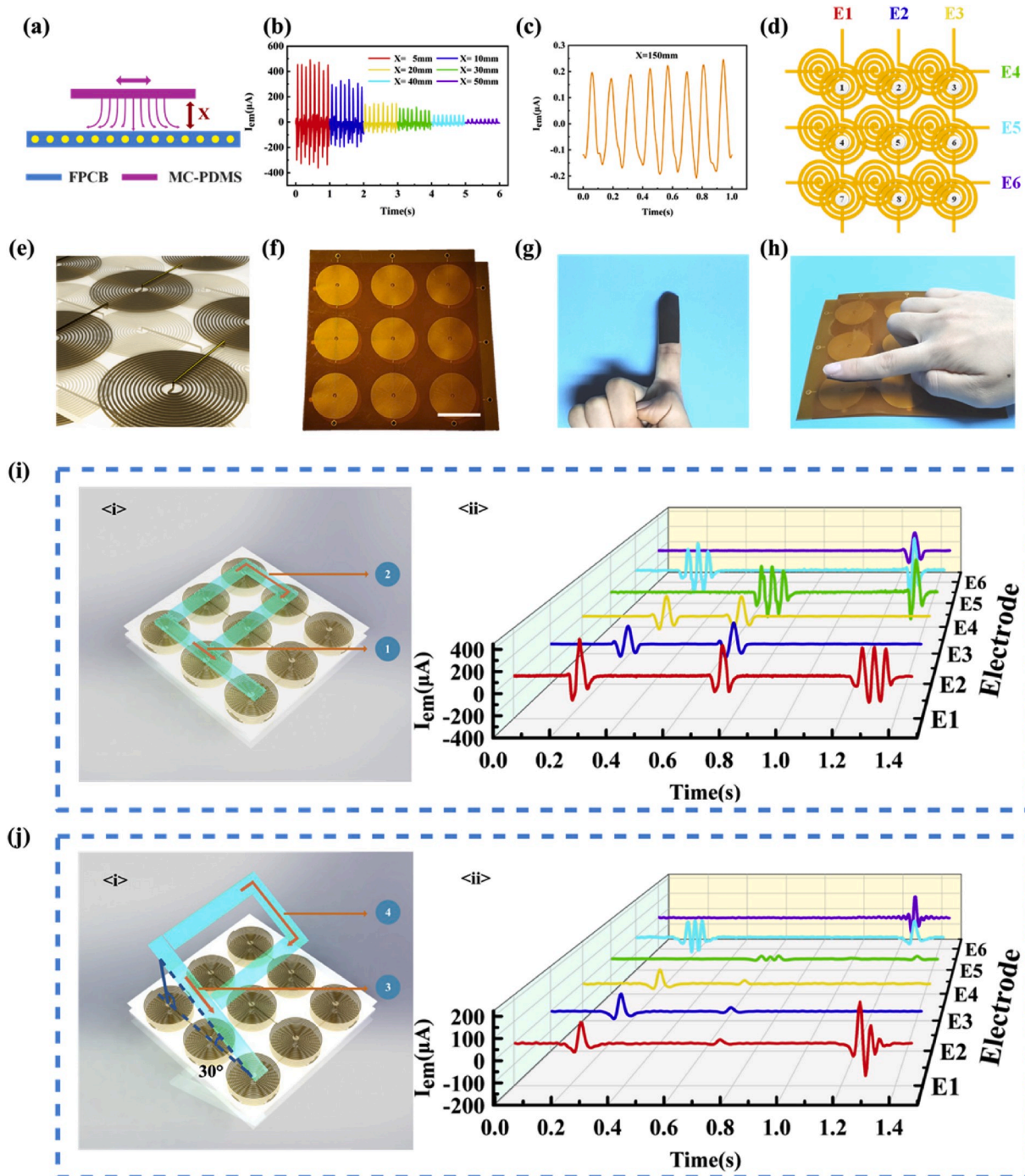


**Fig. 5.** Application of the hybrid generator as a 3D trajectory sensor. (a) Working principle of the 3D trajectory sensing. (b) Output current of the EMG dependent of the X from 5 mm to 50 mm at 4 Hz stimuli. (c) Output current of the EMG when X = 150 mm. (d) Design of the 3 × 3 copper FPCB coil array. (e) Schematic diagram of the details about the coil in series. (f) Image of the customized FPCB coil array, scale bar is 3 cm. (g) Image of MC-PDMS attached to finger. (h) Finger crosses over the copper FPCB coil array. (i) Writing a letter 'P' in a two deminsional plane above the array at a relative stable speed. (j) Writing a letter 'P' in a three dimension space above the array at a relatively stable speed.

Hz low pass filtering as shown in Fig. 5c.

Based on the phenomenon, we designed the copper FPCB coil array in Fig. 5d, which is two pieces superimposed together, each one is composed of nine coils and three of the same row are connected in series making one electrode. The two pieces of array are orthogonal placed so that one electrode of (E1, E2, E3) and one electrode of (E4, E5, E6) can determine a single point in the  $3 \times 3$  array (For example E1 and E4 can locate point 1). Fig. 5e shows that the series process is achieved by drilling technology of FPCB thus the back electrode can make coils conductive to each other, so that the three coil in a row can share the common electrode. Fig. 5f shows the photo of the FPCB array from which the size of the array is  $14 \text{ cm} \times 13.3 \text{ cm}$ .

Based on the array, we demonstrated the trajectory of the MC-PDMS in a two deminsional plane and a three deminsional space. As shown in Fig. 5g, we attached the all-flexible MC-PDMS on a finger firmly which can be used for writing above the FPCB array, whose movement can have megnetoelectricity in the coil, thus they work as a whole EMG as shown in Fig. 5h. Fig. S9a shows the contrast output of the E1 and E2 while the finger slides above the E1 electrode. Electrode E1 outputs a current more than  $200 \mu\text{A}$  while electrode E2 outputs a current less than  $1 \mu\text{A}$ , thus the electromagnetic induced current on the adjacent electrode can be ignored.

As to the recognition of the MC-PDMS's trajectory, for example, in Fig. 5i, we write a letter 'P' right above the coil array at a relative stable speed. The first stroke crossed point 1,4,7 in sequence which can observed by signal of (E1, E4), (E1, E5) and (E1, E6) with the time axis ranging from 1.5s to 1.2s in the schematic diagram Fig. 5i. Since the height of MC-PDMS is stable at about 10 mm above the array, so the single EMG current output is about  $350 \mu\text{A}$ . Then the second stroke of the letter 'P' crossed point 1,2,3,6,5,4 in sequence which can be distinguished by signal of (E1, E4), (E2, E4), (E3, E4), (E3, E5), (E2, E5), (E1, E5) with the time ranging from 1.2s to 0s.

Except that, the output of the EMG can even be utilized for a three dimensional trajectory sensing as shown in Fig. 5j. The MC-PDMS was attached on the finger then a letter 'P' was written over a plane inclined thirty degrees at a relatively stable speed. From Fig. 5j, the third stroke passed point 1,4,7 in sequence which can observed by signal of (E1, E4 at  $20 \mu\text{A}$ ), (E1, E5 at  $100 \mu\text{A}$ ) and (E1, E6 at  $200 \mu\text{A}$ ) with the time axis ranging from 1.5s to 1.2s. It can be explained by the fact that point 1 is about 50 mm above the array, point 4 is about 30 mm above the array and point 7 is about 10 mm above the array. At the same time, the forth stroke crossed point 1,2,3,6,5,4 in sequence, signals will be generated in electrodes like (E1, E4 at  $20 \mu\text{A}$ ), (E2, E4 at  $20 \mu\text{A}$ ), (E3, E4 at  $20 \mu\text{A}$ ), (E3, E5 at  $100 \mu\text{A}$ ), (E2, E5 at  $100 \mu\text{A}$ ), (E1, E5 at  $100 \mu\text{A}$ ) with the time axis ranging from 1.2s to 0s. To sum up, the signal's value can distinguish the trajectory of the MC-PDMS in the Z axis. As a result, when combining the MC-PDMS with the copper FPCB coil array, the EMG part can detect the moving information in a three dimensional space.

### 3. Conclusions

In summary, we have proposed a flexible hybridized electromagnetic-triboelectric nanogenerator for energy harvesting and 3D trajectory sensing. The hybrid generator creatively demonstrates a total flexible, conductive and magnetic PDMS based polymer within several plain fabrication process, which can be used for both electrode of the TENG and the megnet of the EMG. It is an advanced wearable hybridized generator accompanied with the copper FPCB coil that can be attached to cloth and human body firmly. As as a TENG, it has an open-circuit voltage at 103 V, a short-circuit of current at  $7.6 \mu\text{A}$  and a maximum power density at  $7.3 \mu\text{W}/\text{cm}^2$ , as an EMG, it has an open-circuit voltage at 1.37 V, a short-circuit current at 1.03 mA and a maximum power density at  $0.04 \text{ mW}/\text{cm}^2$ . It can charge a capacitance of  $10 \mu\text{F}$  to 3 V in 110 s which is greatly improved by single TENG/EMG configuration. Besides, the EMG is utilized for the 3D trajectory tracking

of the MC-PDMS attached to the finger which can not only recognize in-plane trajectory but also the out-of-plane height information. Therefore, with the flexible multi-functional material, this hybridized generator is a promising candidate in the wearable energy devices and a great innovation in the 3D trajectory recognition in human-machine fields.

## 4. Experimental section

### 4.1. Fabrication of MC-PDMS

The MC-PDMS is composed of PDMS, MWCNT and NdFeB with the weight ratio of 1: 0.07: 5 which is mixed by the cosolvent toluene, and the magnetization is finished by a pulsed magnetizer (DPM1, euSCI Co., China). In details, first 5 g PDMS base resin (Sylgard 184, Dow Corning Co., USA) is dissolve with 15 ml toluene along with 350 mg MWCNT (diameter: 10–20 nm, length: 10–30  $\mu\text{m}$ , purity >98%, Boyu, Co.) and 25 g NdFeB (MQFP-B D50 = 5  $\mu\text{m}$ , Magnequench Co.), which is stirred vigorously for 4 h at room temperature in a closed conical bottle until the uniform black viscous liquid is achieve. Then 0.5 g PDMS cross-linker is added under stirring in an open environment for the fully evaporation of the toluene, after which the final liquid is filled into the prepared PMMA mold and kept at  $80 \text{ }^\circ\text{C}$  for 2 h, thus after the pulsed magnetization, the bulk NdFeB and MWCNT doped PDMS is achieved.

### 4.2. Characterization and measurement

Morphologies of the MC-PDMS are observed using Scanning electron microscopy (SEM, Quanta 600F, FEI Co.) with an operation voltage of 5 kV. Images of MC-PDMS's magnetic domain is taken by Atomic force microscope (AFM, BRUKER NANO INC.). Resistance and magnetic induction intensity are characterized by a multimeter and a gauss meter respectively. Besides, for the electrical signal responses, the current outputs are amplified by a SR570 low-noise current preamplifier and the voltage outputs are amplified by a SR560 low-noise voltage preamplifier from Stanford Research Systems and measured via a digital oscilloscope (Agilent DSO-X 2014A).

### Declaration of competing interest

The authors declare no conflict of interest.

### CRediT authorship contribution statement

**Ji Wan:** Conceptualization, Data curation, Formal analysis, Writing - original draft, Writing - review & editing, Investigation, Software, Methodology. **Haobin Wang:** Software, Investigation, Writing - review & editing. **Liming Miao:** Conceptualization, Writing - review & editing. **Xuexian Chen:** Writing - review & editing. **Yu Song:** Writing - review & editing. **Hang Guo:** Visualization. **Chen Xu:** Validation. **Zhongyang Ren:** Resources. **Haixia Zhang:** Conceptualization, Methodology, Resources, Writing - review & editing, Supervision, Project administration, Funding acquisition.

### Acknowledgements

The authors thank Dr. Hao-tian Chen from École Polytechnique Fédérale de Lausanne (EPFL) for guiding experiment and polishing language and Mu-chan Li from Peking University for AFM tests. This work was supported by National Key R&D Project from Minister of Science and Technology, China (2016YFA0202701) and the National Natural Science Foundation of China (Grant No. 61674004).

### Appendix A. Supplementary data

Supplementary data to this article can be found online at <https://doi.org/10.1016/j.nanoen.2020.104878>.

## References

- [1] X. Cheng, B. Meng, X. Zhang, M. Han, Z. Su, H. Zhang, *Nano Energy* 12 (2015) 19–25.
- [2] W. Tang, Y. Han, C. Han, C. Gao, X. Cao, Z. Wang, *Adv. Mater.* 27 (2015) 272–276.
- [3] B. Meng, W. Tang, Z. Too, X. Zhang, M. Han, W. Liu, H. Zhang, *Energy Environ. Sci.* 6 (2013) 3235–3240.
- [4] Y. Song, H. Wang, X. Cheng, G. Li, X. Chen, H. Chen, L. Miao, X. Zhang, H. Zhang, *Nano Energy* 55 (2019) 29–36.
- [5] Z. Wang, T. Jiang, L. Xu, *Nano Energy* 39 (2017) 9–23.
- [6] B. Chen, W. Tang, C. He, C. Deng, L. Yang, L. Zhu, J. Chen, J. Shao, L. Liu, Z. Wang, *Mater. Today* 21 (2018) 88–97.
- [7] H. Zou, Y. Zhang, L. Guo, P. Wang, X. He, G. Dai, H. Zheng, C. Chen, A. Wang, C. Xu, Z. Wang, *Nat. Commun.* 10 (2019) 1427.
- [8] S. Niu, S. Wang, L. Lin, Y. Liu, Y. Zhou, Y. Hu, Z. Wang, *Energy Environ. Sci.* 6 (2013) 3576–3583.
- [9] B. Chen, W. Tang, C. Zhang, L. Xu, L. Zhu, L. Yang, C. He, J. Chen, L. Liu, T. Zhou, Z. Wang, *Nano Res.* 11 (6) (2018), 3096–3015.
- [10] X. Zhang, M. Han, R. Wang, B. Meng, F. Zhu, X. Sun, W. Hu, W. Wang, Z. Li, H. Zhang, *Nano Energy* 4 (2014) 123–131.
- [11] S. Wang, L. Lin, Y. Xie, Q. Jing, S. Niu, Z. Wang, *Nano Lett.* 13 (2013) 2226–2233.
- [12] X. Zhang, M. Han, R. Wang, F. Zhu, Z. Li, W. Wang, H. Zhang, *Nano Lett.* 13 (2013) 1168–1172.
- [13] S. Niu, Y. Liu, S. Wang, L. Lin, Y. Zhou, Y. Hu, Z. Wang, *Adv. Funct. Mater.* 24 (2014) 3332–3340.
- [14] M. Yeh, H. Guo, L. Lin, Z. Wen, Z. Li, C. Hu, Z. Wang, *Adv. Funct. Mater.* 26 (2016) 1054–1062.
- [15] B. Chen, W. Tang, T. Jiang, L. Zhu, X. Chen, C. He, L. Xu, H. Guo, P. Lin, D. Li, J. Shao, Z. Wang, *Nano Energy* 45 (2018) 380–389.
- [16] Z. Wang, J. Song, *Science* 312 (2006) 242–246.
- [17] G. Zhu, A. Wang, Y. Liu, Y. Zhou, Z. Wang, *Nano Lett.* 12 (2012) 3086–3090.
- [18] Y. Hu, Y. Zhang, C. Xu, L. Lin, R. Snyder, Z. Wang, *Nano Lett.* 11 (2011) 2572–2577.
- [19] M. Han, X. Zhang, B. Meng, W. Liu, W. Tang, X. Sun, W. Wang, H. Zhang, *ACS Nano* 7 (2013) 8554–8560.
- [20] X. Chen, H. Guo, H. Wu, H. Chen, Y. Song, Z. Su, H. Zhang, *Nano Energy* 49 (2018) 51–58.
- [21] Y. Chen, Y. Cheng, Y. Jie, X. Cao, N. Wang, Z. Wang, *Energy Environ. Sci.* 12 (2019) 2678–2684.
- [22] Z. Wu, H. Guo, W. Ding, Y. Wang, L. Zhang, Z. Wang, *ACS Nano* 13 (2019) 2349–2356.
- [23] X. Fan, J. He, J. Mu, J. Qian, N. Zhang, C. Yang, X. Hou, W. Geng, X. Wang, X. Chou, *Nano Energy* 68 (2020) 104319.
- [24] J. He, X. Fan, J. Mu, C. Wang, J. Qian, X. Li, X. Hou, W. Geng, X. Wang, X. Chou, *Energy* 194 (2020) 116871.
- [25] X. Wang, Z. Wang, Y. Yang, *Nano Energy* 26 (2016) 164–171.
- [26] H. Shao, Z. Wen, P. Cheng, N. Sun, Q. Shen, C. Zhou, M. Peng, Y. Yang, X. Xie, X. Sun, *Nano Energy* 39 (2017) 608–615.
- [27] Z. Ren, Q. Zheng, H. Wang, H. Guo, L. Miao, J. Wan, C. Xu, S. Cheng, H. Zhang, *Nano Energy* (2019) 104243.
- [28] C. Zhang, W. Tang, C. Han, F. Fan, Z. Wang, *Adv. Mater.* 26 (2014) 3580–3591.
- [29] K. Zhang, X. Wang, Y. Yang, Z. Wang, *ACS Nano* 9 (2015) 3521–3529.
- [30] T. Quan, X. Wang, Z. Wang, Y. Yang, *ACS Nano* 9 (2015) 12301–12310.
- [31] Y. Chen, D. Liu, S. Wang, Y. Li, X. Zhang, *Nano Energy* 64 (2019) 103911.
- [32] B. Meng, W. Tang, X. Zhang, M. Han, W. Liu, H. Zhang, *Nano Energy* 2 (2013) 1101–1106.
- [33] H. Chen, Y. Song, H. Guo, L. Miao, X. Chen, Z. Su, H. Zhang, *Nano Energy* 51 (2018) 496–503.
- [34] H. Chen, Y. Song, X. Cheng, H. Zhang, *Nano Energy* 56 (2019) 252–268.
- [35] X. Zhang, M. Han, B. Kim, J. Bao, J. Brugger, H. Zhang, *Nano Energy* 47 (2018) 410–426.
- [36] H. Chen, L. Miao, Z. Su, Y. Song, M. Han, X. Chen, X. Cheng, D. Chen, H. Zhang, *Nano Energy* 40 (2017) 65–72.
- [37] B. Chen, W. Tang, C. He, T. Jiang, L. Xu, L. Zhu, G. Gu, J. Chen, J. Shao, J. Luo, Z. Wang, *Adv. Mater. Technol.* 3 (2017) 1700229.
- [38] M. Shi, J. Zhang, H. Chen, M. Han, S. Shankaregowda, Z. Su, B. Meng, X. Cheng, H. Zhang, *ACS Nano* 10 (2016) 4083–4091.
- [39] H. Wu, Z. Su, M. Shi, L. Miao, Y. Song, H. Chen, M. Han, H. Zhang, *Adv. Funct. Mater.* 28 (2018) 1704641.
- [40] H. Guo, H. Wu, Y. Song, L. Miao, X. Chen, H. Chen, Z. Su, M. Han, H. Zhang, *Nano Energy* 58 (2019) 121–129.
- [41] L. Lin, Y. Xie, S. Wang, W. Wu, S. Niu, X. Wen, Z. Wang, *ACS Nano* 7 (2013) 8266–8274.
- [42] X. Wang, H. Zhang, L. Dong, X. Han, W. Du, J. Zhai, C. Pan, Z. Wang, *Adv. Mater.* 28 (2016) 2896–2903.
- [43] C. Han, C. Zhang, X. Li, L. Zhang, T. Zhou, W. Hu, Z. Wang, *Nano Energy* 9 (2014) 325–333.



**Ji Wan** received the B.S. degree from Peking University in 2019. He is currently pursuing the Ph.D degree at School of Electronics Engineering and Computer Science, Peking University, Beijing, China. His research interests mainly include self-powered electronic skin and composite materials.



**Haobin Wang** received the B.S. degree from Jilin University, Changchun, in 2018. He is currently pursuing the Ph.D. degree at the National Key Laboratory of Nano/Micro Fabrication Technology, Peking University, Beijing, China. His research interests mainly include micro-supercapacitors and the integration of self-charging system.



**Liming Miao** received the B.S. degree from Peking University, Beijing, in 2017. His research interests mainly include wrinkle structure and triboelectric nanogenerator.



**Xuexian Chen** received the B.S. degree from the University of Electronic Science and Technology of China, Chengdu, in 2015. She is currently pursuing the Ph.D. degree at the National Key Laboratory of Nano/Micro Fabrication Technology, Peking University, Beijing, China. Her research interests mainly include design and fabrication of hybrid nanogenerator and electrospinning process.



**Yu Song** received the B.S. degree in Electronic Science & Technology from Huazhong University of Science and Technology, China, in 2015. He is currently pursuing the Ph.D. degree at the National Key Laboratory of Nano/Micro Fabrication Technology, Peking University, Beijing, China. He majors in MEMS and his research is focusing on supercapacitors and self-charging power system.



**Hang Guo** received his B.S. degree from Huazhong University of Science and Technology (HUST) in 2017 and now is a Ph.D. student at Academy for Advanced Interdisciplinary Studies in Peking University. His research interests focus on electronic skin and self-powered nanosystems.



**Zhongyang Ren** received the B.E. degree from FuZhou University, FuZhou, in 2017. And then he pursuing the M.E. degree at FuZhou University, and also as a joint student at the National Key Laboratory of Nano/Micro Fabrication Technology, Peking University, Beijing, China. His research interests mainly include optoelectronic materials and devices and the hybrid energy harvester.



**Chen Xu** received the B.S. degree from Beijing Institute of Technology in 2019. He is currently pursuing the Ph.D degree at Academy for Advanced Interdisciplinary Studies, Peking University, Beijing, China. His research interests mainly include flexible sensors and self-powered nanosystems.



**Hai-Xia (Alice) Zhang (SM'10)** received the Ph.D. degree in mechanical engineering from Huazhong University of Science and Technology, Wuhan, China, 1998. She is currently a Professor with the Institute of Microelectronics, Peking University, Beijing, China. She joined the faculty of the Institute of Microelectronics in 2001 after finishing her post-doctoral research in Tsinghua University. Her research interests include MEMS design and fabrication technology, SiC MEMS, and micro energy technology. She has served on the General Chair of the IEEE NEMS 2013 Conference, the Organizing Chair of Transducers' 11. As the Founder of the International Contest of Applications in Network of things, she has been organizing this world-wide event since 2007. In 2006, she received the National Invention Award of Science and Technology.